

DOI: 10.1002/((please add manuscript number))

Article type: Full Paper

Stretchable Thermoplastic Elastomer Optical Fibers for Sensing of Extreme Deformations

*Andreas Leber, Beth Cholst, Joseph Sandt, Nicolas Vogel & Mathias Kolle**

A. Leber, B. Cholst, J. Sandt, Prof. M. Kolle

Department of Mechanical Engineering, Massachusetts Institute of Technology, 77 Massachusetts Avenue, Cambridge, MA 02139-4301, USA

E-mail: mkolle@mit.edu

A. Leber, Prof. N. Vogel

Institute of Particle Technology, Friedrich-Alexander University Erlangen-Nürnberg, Schlossplatz 4, 91054 Erlangen, Germany

Keywords: stretchable optical fibers, human motion tracking, textile-based sensors, thermoplastic elastomers, soft optical materials

The design of advanced materials with coupled optical and mechanical properties is an important challenge in materials science; especially, the implementation of soft materials in optics has recently gained significant interest. Soft optical systems are particularly versatile in sensing, where large and repeated deformations require dynamically responsive materials. Here, stretchable step-index optical fibers, which are capable of reversibly sustaining strains of up to 300% while guiding light, are demonstrated. A continuous and scalable melt-flow process is used to co-extrude two thermoplastic elastomers, thereby forming the fibers' high index core-low index cladding structure. Deformation of the fibers through stretching, bending, and indentation induces detectable, predictable, reversible, and wavelength-dependent changes in light transmission. Quantitative knowledge about the coupling of the fibers' mechanical and optical properties forms the basis for the design of fiber-based sensors that are capable of reliably assessing extreme mechanical stimuli. The fibers utility in sensing scenarios is demonstrated in a knee brace for continuous knee motion tracking, a glove for

This is the author manuscript accepted for publication and has undergone full peer review but has not been through the copyediting, typesetting, pagination and proofreading process, which may lead to differences between this version and the [Version of Record](#). Please cite this article as [doi: 10.1002/adfm.201802629](#).

This article is protected by copyright. All rights reserved.

control of a virtual hand model, and a tennis racket capable of locating ball impacts. Such devices could greatly improve quantitative assessment of human motion in rehabilitation, sports, and anywhere else where large deformations need to be monitored reliably.

1. Introduction

Wearable functional textiles enable the detection of deformations induced by human body motion for a wide range of applications in health monitoring, sports, and human-machine interaction.^[1–8] A significant challenge in these applications arises from the large range of deformations that functional textiles must tolerate to reliably follow the movement of the human body.

Advances in device materials and structure have fueled the development of electronic textile sensors that exploit a variety of resistive,^[9,10] capacitive,^[11–13] and inductive^[14] detection strategies. However, materials with vastly different mechanical properties, electronic behavior, and processing attributes must be combined in these sensors to maintain adequate performance upon large and repeated deformations. This often necessitates complex manufacturing processes.^[9–12] Examples include the deposition of conductive nanoscale components, such as carbon nanotubes^[9] or silver nanowires^[10], onto deformable poly(dimethylsiloxane) (PDMS) substrates, injection of liquid metal gallium indium into elastomeric polyester hollow fibers,^[12] and the stacking of compliant silver-plated knitted textile and PDMS layers^[11].

A promising alternative strategy for the design of textiles that monitor body motion relies on the use of optical fibers integrated into functional fabrics. Optical fibers can be formed from two transparent materials that have similar mechanical properties and processing behavior but differ in refractive index. They are arranged in a simple core-cladding morphology.^[15] While standard optical fiber

materials such as silica glass and polymethylmethacrylate (PMMA) are rigid and allow only for small deformations^[16], alternative optical fiber materials including elastomers^[17–19] and hydrogels^[20,21] have been investigated for use in mechanically demanding settings. These efforts demonstrate the potential of deformable optical fibers for sensing of large strains. However, fiber samples were only produced in laboratory-scale quantities as the reported fabrication processes are not compatible with scalable fiber manufacturing strategies. Specifically, the fabrication of these soft fibers involves the injection of polymer precursors into a mold, followed by chemical crosslinking and demolding, posing severe restrictions on the achievable fiber length and ultimately the throughput of this technique. For this reason, recent efforts have focused on physically crosslinked thermoplastic elastomers, which are highly deformable and compatible with high-throughput melt-processing methods.^[22–25] While early results show great promise, a truly scalable manufacturing process of stretchable core-cladding thermoplastic elastomer optical fibers has not been developed. Furthermore, fibers that provide persistent sensing functionality for strains exceeding 100% under repeated deformation have yet to be demonstrated. Reliable performance at such high levels of strain is desirable for integrated textile sensors and for quantitative monitoring of human body and tissue dynamics.

Here, we report the design and scalable manufacture of highly stretchable and flexible optical fibers. We take advantage of the melt-processability of thermoplastic elastomers and employ a one-step, continuous co-extrusion process to fabricate optical fibers at a scale of several hundred meters of fiber in one hour. Comparable to conventional optical fibers made of glass or thermoplastics, the fibers presented here guide light by total internal reflection occurring at the interface of their high refractive index core ($n_{\text{core}} = 1.52$) and low refractive index cladding ($n_{\text{cladding}} = 1.36$). The fibers are

highly deformable, sustaining extreme elongation, bending, and indentation. Moreover, the different types of fiber deformation induce detectable, predictable, reversible, and wavelength-dependent changes in light transmission. This opto-mechanical coupling forms the basis for a fiber-based sensor capable of quantifying extreme mechanical stimuli. We demonstrate reliable and durable deformation detection for axial strains of up to 300%, which has never before been demonstrated for optical fibers.

To elucidate the potential of the fibers in body monitoring and integrated textile sensors, we present several device prototypes that combine the fibers with low-cost electronic components: (1) a knee brace for continuous monitoring of knee angle during sports or rehabilitation exercise; (2) a glove capable of tracking finger movement to control a virtual hand model; (3) a tennis racket capable of locating ball impacts.

2. Results and discussion

2.1. Fabrication of stretchable optical fibers

The growing interest in stretchable optical fibers and the need of large fiber lengths for functional textiles is best met by high-throughput melt-processing techniques. Suitable raw materials must be melt-processable and highly deformable, two properties which are both found in thermoplastic elastomers. Optical criteria limiting materials selection are a well-defined refractive index contrast between the core and the cladding to ensure light guiding by total internal reflection and a high transparency for low-loss light transmission. With these requirements in mind, we evaluated several commercially available thermoplastic elastomers with satisfactory reported melt-processing compatibility and optical transparency as candidates for the fiber materials. The primary two metrics

that we employed were the materials' refractive index and the elongation at break as a measure of mechanical performance (**Figure 1a**). Out of 10 different commercial thermoplastic elastomers that we considered, we selected the polystyrene-based polymer Star Clear 1044 (refractive index $n=1.52$, elongation at break $\epsilon_{\max} = 693\%$) as the core material and the fluorinated polymer Daikin T-530 ($n = 1.36$, $\epsilon_{\max} = 580\%$) for the cladding. The two materials have a large contrast in refractive index, which is important for light guiding in fibers. They also exhibit a similar mechanical performance reflected in comparable stress-strain curves (Supporting Information, Figure S1), which helps in reducing mechanical mismatch and potential mechanical failure during manufacture and subsequent application.

To form optical fibers from the chosen materials, we devised a co-extrusion process (**Figure 1b**). The setup consists of two single-screw extruders that feed the polymer melt into a custom-made concentric co-extrusion nozzle to form the core-cladding structure. Down-stream of the extrusion nozzle, the fiber is cooled by the surrounding air and taken up by a spool. The diameter of the fiber can be tuned by adjusting the speed of the take-up spool relative to the extrusion speed, as the temperature of the fiber is still within the processing window immediately after being forced out of the nozzle. Outer diameters ranging from 0.5mm to 3mm were fabricated reliably. In accordance with the industry standard for step-index polymer optical fibers,^[26] the diameter was set to 1mm for the fibers reported in this work. The fabrication of 200m of fiber in one hour illustrates the scale-up potential of this one-step continuous co-extrusion process (**Figure 1c**).

The extruded fibers guide light and can be tied into knots (**Figure 1d**), qualitatively demonstrating their optical performance and mechanical resilience. The fibers' core-cladding structure was visualized by examination of a fiber end face with an optical microscope, while red light was coupled

in at the other fiber end (Figure 1e). The emission of red light predominantly from the core indicates light guiding by total internal reflection. The core and the cladding are not fully concentric, which is caused by an asymmetry in the co-extrusion nozzle and can easily be addressed in future design iterations. Nonetheless, the cladding fully surrounds the core along the fiber, thus enabling continuous light guiding.

Insights into the fibers' strain-dependent light guiding characteristics are provided by stretching the fibers to multiples of their initial length (Figure 1f). Elongation results in a spectrally-varying attenuation of light, which is evident in the color variation of side-emitted light along the stretched fiber from white to red.

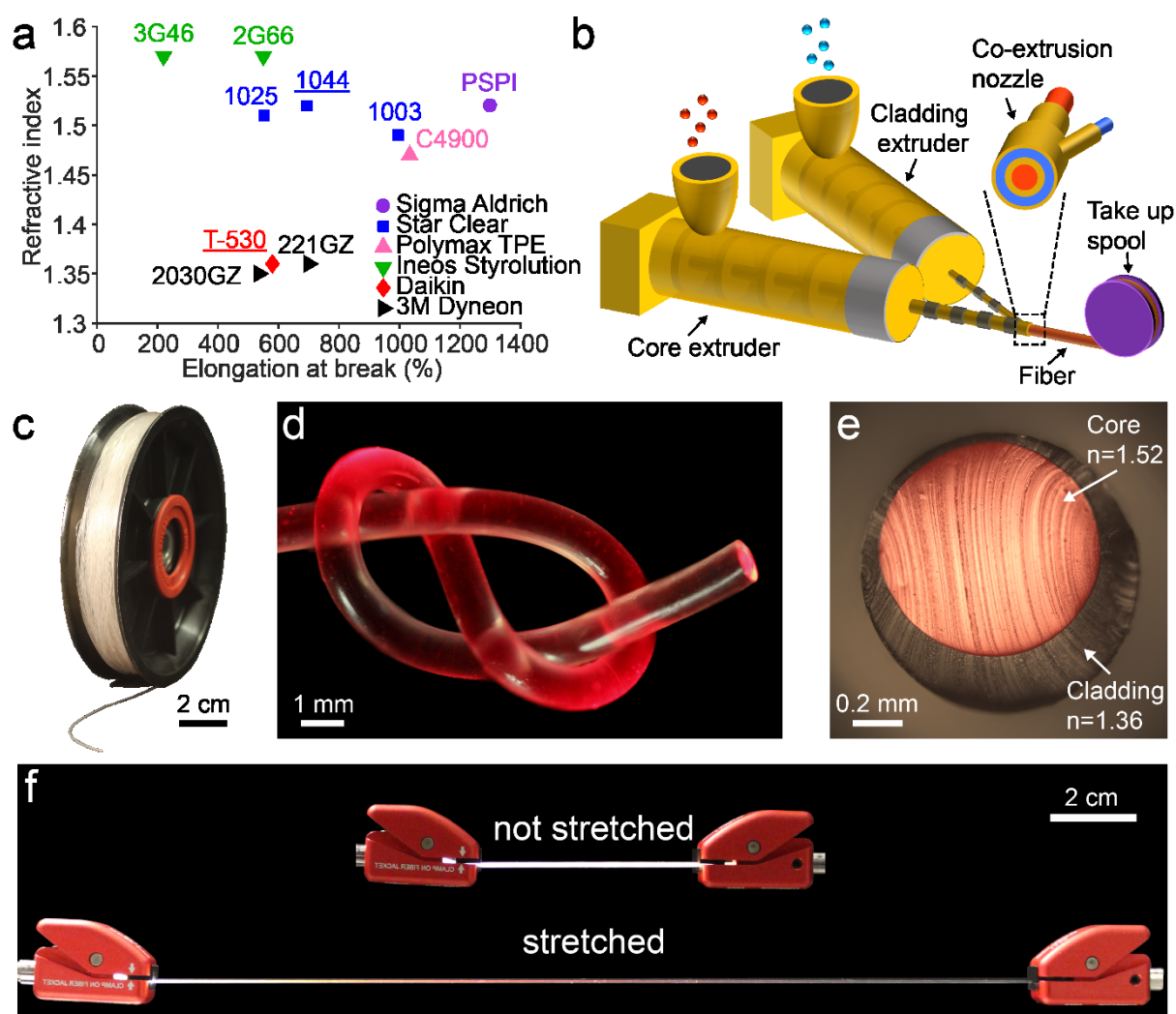


Figure 1. Materials, fabrication, and structure of the fibers. (a) Comparison of elongation at break and refractive index of melt-processable and light-transmitting thermoplastic elastomers. The selected polymers (Star Clear 1044 and Daikin T-530) are underlined. (b) Schematic of the one-step co-extrusion fabrication of stretchable step-index optical fibers. (c) Roll of 200m of fiber fabricated in one hour. (d) A fiber guiding light is tied into a knot. (e) Optical micrograph of a fiber end face. Red light coupled in at the opposite fiber end is emitted predominantly from the core, illustrating light guiding by total internal reflection. The cladding is only visible due to external illumination with white light by the microscope for better visualization of the fiber architecture. (f) A fiber guides light while it is stretched to four times its original length. The spectrally varying attenuation of light can be seen by the variation of side-emitted color.

2.2. Mechanical and optical properties

To assess the fibers' mechanical and optical properties quantitatively, we separately performed tensile testing experiments and spectroscopic analysis of transmitted light.

The core-cladding fibers maintain their mechanical integrity for strains of up to $545 \pm 35\%$, at which point both materials fail simultaneously (**Figure 2a**). This failure strain is comparable to standard Spandex filament, which commonly breaks between 450% and 700%.^[27] Additionally, we determined a 100% modulus of 0.76 ± 0.05 MPa and a failure stress of 10.66 ± 1.88 MPa. We also tested the mechanical behavior of the fibers under cyclic loading. A fiber was stretched and relaxed repeatedly between 0% and 300% strain for up to 100 cycles (Supporting Information, Figure S2). While the fiber exhibited a predominantly elastic response, a plastic deformation of 17% after the first cycle up to 34% after 100 cycles was found. This plastic behavior could potentially reduce the fibers' utility in sensing applications. To address this limitation, the fiber was pre-stretched to 40% initial strain and the experiment was repeated at cyclic strains of 40% - 300% (Figure 2b). In this experiment, the fiber's behavior appeared entirely elastic, remaining taut for the complete strain range and number of cycles considered. Additionally, in both experiments, hysteresis and stress softening between cycle 1 and 10 were observed. This softening effect during the first few cycles is also referred to as the Mullins effect and has been extensively studied for elastomeric materials^[28], including thermoplastic elastomers^[29].

To characterize the fibers' optical performance, we quantified their propagation losses by sequentially shortening them and measuring the transmitted light intensity, a procedure known as the cutback method^[26]. At all wavelengths, the intensity of transmitted light increased exponentially with decreasing fiber length (Figure 2c, d), following the Beer-Lambert law. We extracted the wavelength-dependent attenuation coefficient from the slope of a linear fit to the logarithmic

propagation loss as a function of fiber length (Figure 2e). In the range of 400 nm – 855 nm, the fiber is less transmissible at shorter wavelengths (1.2 dB cm^{-1} at 400 nm) than at longer wavelengths (0.8 dB cm^{-1} at 855 nm). The determined attenuation coefficient corresponds to values reported for other stretchable optical fibers,^[18,20–25] but is three orders of magnitude larger than standard PMMA optical fibers.^[30] Presumably, the observed losses are caused by defects present within the core or at the core-cladding interface, such as particle inclusions, voids, or inhomogeneous core diameters. Light is scattered at such defects, resulting in leakage (Figure 1d, f). Step-index optical fibers that include a significant number of defects are known to exhibit a dependence of their light transmission characteristics on the surrounding medium.^[21,31] This is attributed to light escaping from the core and being guided within the cladding in a low refractive index surrounding medium but being completely coupled out of the fiber in a high refractive index medium.^[21] To test the effectiveness of the cladding in variable environments, we compared our core-cladding fibers to core-only fibers in air ($n \approx 1.00$), deionized water ($n \approx 1.33$), and silicon oil ($n \approx 1.40$) (Figure 2f). As expected, the transmission through fibers without a low-index cladding decreased significantly as the refractive index of the surrounding medium increased, which is a major limitation for applications. In contrast, the core-cladding fibers showed persistent light guiding performance with a negligible dependency on the medium surrounding the fibers. Thus, the stretchable core-cladding fibers can be employed in variable settings with fiber performance being nearly unaffected by surface contaminations or changes in the surrounding medium.

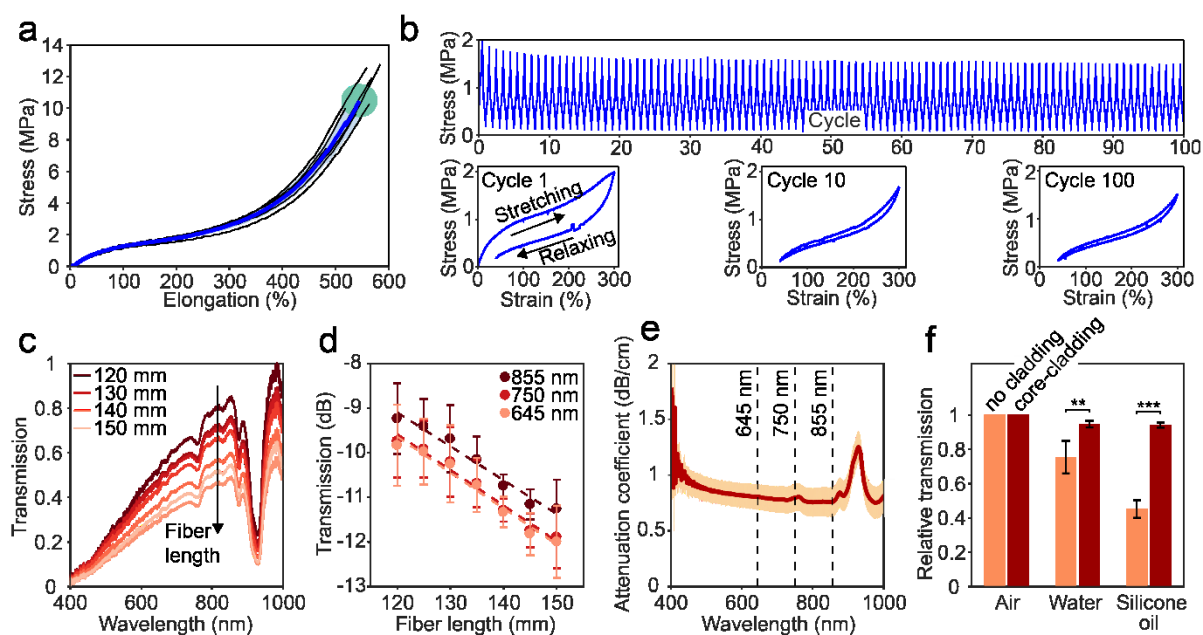


Figure 2. Mechanical and optical properties of the fibers. (a) Stress-strain curve of fibers obtained through tensile testing. The thin black lines are the curves for individual samples. The mean and standard deviation are represented by the thick blue line and the blue shaded area, respectively. The green shaded ellipse marks the standard deviation of the elongation and stress at break. (b) Dynamic tensile test of a fiber being stretched over 100 cycles in the range of 40% - 300%, showing elastic behavior. (c) Transmission spectra at various fiber lengths normalized to the maximum intensity of the fiber with the highest transmission. (d) Transmission at wavelengths 645 nm, 750 nm, and 855 nm as a function of fiber length. (e) Attenuation coefficient of the fibers as a function of wavelength. The red line represents the mean, while the orange shaded area represents the standard deviation. The wavelengths considered in the following analysis of deformation-induced transmission losses are marked as dashed lines. (f) Light-guiding properties of pure core and core-cladding fibers in different surrounding media. Light transmission in air, water, and oil is only equivalent in the presence of a cladding.

2.3. Deformation sensing

Having assessed the fibers' mechanical and optical properties separately, the most important question remains to be addressed: How do deformations applied to the stretchable core-cladding fibers affect their light transmission characteristics? The quantitative answer to this question

presented below forms the foundation for the development of optical fiber-based deformation sensors. In the following, we provide a detailed discussion of the fibers' wavelength-dependent optical response to perturbations caused by repeated stretching, bending, and indentation to magnitudes of deformation that would not be reversibly supported by the majority of materials used in optical design, including polymeric components such as PMMA.^[32]

To quantify the impact of stretching on the fibers' light transmission characteristics, fibers were repeatedly extended and relaxed within the strain range of 40% - 300%, while simultaneously monitoring the intensity of transmitted light at wavelengths 645 nm, 750 nm, and 855 nm (**Figure 3a**). The fibers exhibited a decrease in transmission upon elongation, which is dependent on wavelength, as well as reversible and repeatable for at least 100 cycles. Transmission losses were larger for shorter wavelengths, in agreement with the wavelength-dependent attenuation coefficient measured in the cutback experiment (Figure 2e). In both the cutback and the stretching experiment, fiber transmission was reduced for increasing fiber lengths due to the longer path of the light through the attenuating medium, an effect that has also been observed in other stretchable optical fibers^[21,25].

The fibers were also repeatedly subjected to controlled bending and indentation, two additional stimuli important in sensing applications (Figure 3b, c). For the bending response assessment, the fibers were bent to the minimum attainable radius of curvature at which fiber sections on either side of the bend are parallel and in contact (defined as a bending radius of zero). In the indentation experiments, fibers were subjected to local indentations up to a depth of 0.625mm (62.5% of the fiber diameter). Similar to the effects of fiber stretching, both types of deformation induced transmission losses that corresponded to the magnitude of deformation. However, in contrast to

stretching, the bending or indenting of the fibers caused a decrease in transmission that was not significantly dependent on the wavelength of transmitted light. Based on this finding, we hypothesize that the observed transmission losses are caused by a failure of propagating light to meet the critical angle requirement for total internal reflection, a well-known effect for optical fibers.^[32]

In accordance with the stress softening discussed in the mechanical characterization (Figure 2b), the transmission loss induced by stretching changed slightly during the first few cycles. However, beyond cycle 10, the fibers exhibited high reversibility in their response to deformation and the loading-unloading cycles only showed a small amount of hysteresis. For the full range of all three modes of deformation shown in Figure 3, the maximum deviation throughout cycles due to hysteresis was determined to be 5% strain, 0.6mm bending radius, and 0.1mm indentation depth (Supporting Information, Figure S3). The uncertainty originating from fluctuations in the transmission for a fiber in the relaxed state or at any fixed degree of deformation fell well below the hysteresis error (1% strain, 0.5mm bending radius, 0.01mm indentation depth – see Figure S4 in Supporting Information). Regarding deformation range, resolution, and hysteresis, the fibers discussed here compare very favorably to optical fiber-based deformation sensors reported previously in the literature (see Table S1 in Supporting Information).

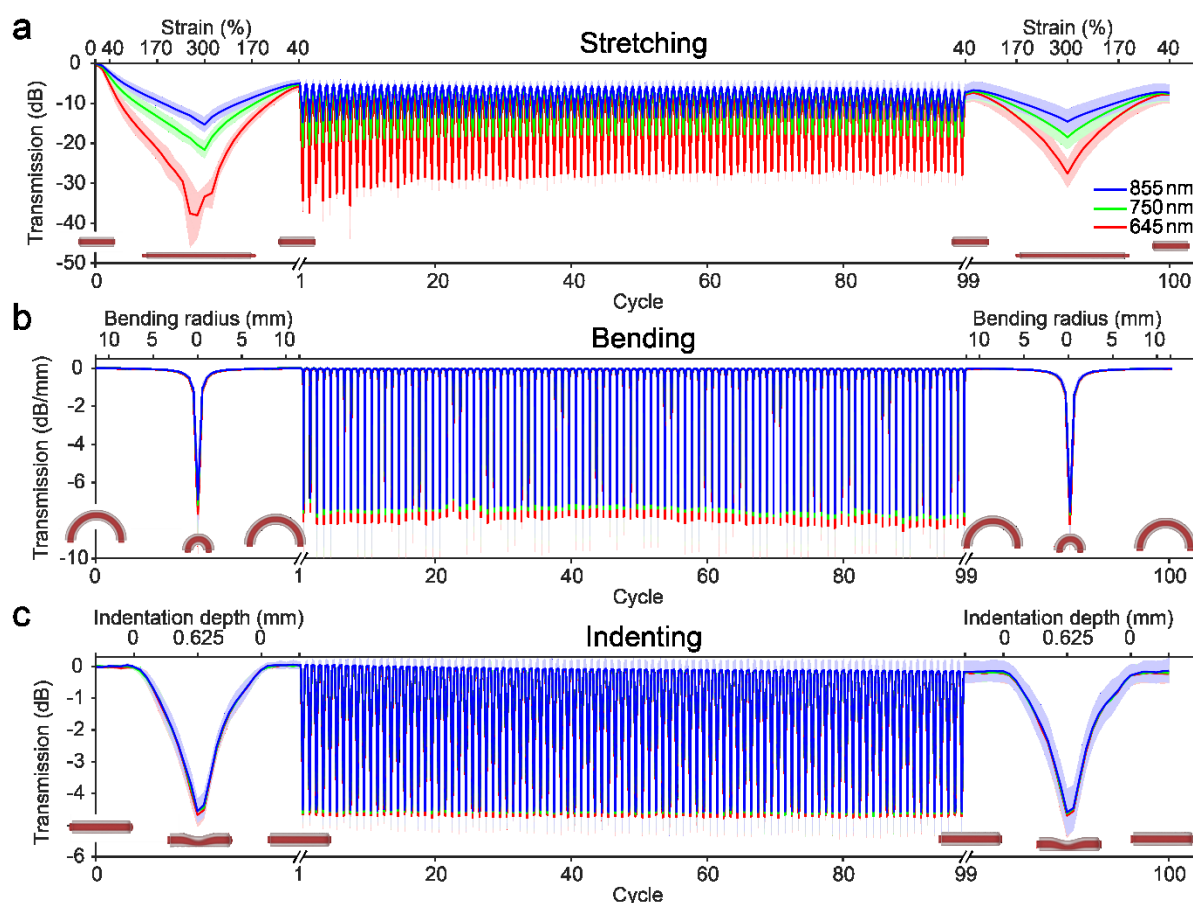


Figure 3. Fibers for deformation sensing. Transmission in fibers for wavelengths 645 nm (red trace), 750 nm (blue trace), and 855 nm (green trace) as a function of cyclical (a) elongation, (b) bending, and (c) indentation. For deformation by bending, the transmission is normalized by the length of the bent fiber section. The lines represent the mean while shaded areas represent the standard deviation of the measurements. The plots of cycle 1 and 100 are expanded to visualize the effect of the magnitude of deformation. The cycles 2-99 are compressed to demonstrate the reversibility and repeatability of deformation-induced transmission losses. The deformation mode is schematically illustrated in the data for cycles 1 and 100.

2.4. Human activity monitoring

Having quantified the fibers' optical response to stretching, bending, and indentation, we hypothesized that sensing devices could take benefit of these different modes of stimulation. We prototyped three types of devices to demonstrate the fibers versatility in kinematic sensing

scenarios where large deformations are expected: a knee brace that monitors the knee angle continuously and in real time; a glove that detects movement of all five fingers and enables real-time control of a virtual hand model; and a tennis racket that provides feedback on ball impact location.

The working principle of all three proposed sensing systems relies on the monitoring of the intensity levels of light that is transmitted through deformable optical fibers. We selected a working wavelength of 645 nm, at which stretching causes a pronounced optical response but never results in complete loss of signal for fiber lengths and strains of interest in the applications. For each system, we used low-cost, standardized, and commonly available electrical components to build a stand-alone, wirelessly-communicating mechanical sensing device.

The knee brace for monitoring human knee joint movement features one fiber, which is fixed atop the knee and is stretched as the knee is bent (**Figure 4a**). Light from a LED of constant brightness is guided by the stretch-sensitive fiber to a photodiode, which outputs a signal proportional to the transmitted light intensity. To verify the functioning of the sensor, we used visual motion tracking to measure the true knee angle. We found an approximately linear decrease of sensor output voltage as a function of knee flexion (Figure 4b). The correlation is ideal, as a narrow window of readout voltages (1.5V - 3.5V) is sufficient to precisely determine the entire motion range of the knee (80° - 180°) without extensive data processing. Moreover, the device can be calibrated on-site using only two visually estimated knee angles (90° and 180° were used in the subsequent tests). This allows us to track and visualize the knee angle in real-time with low computational effort, in contrast to visual motion tracking, where either computationally intensive real-time feature recognition and tracking algorithms are required, or post-experiment data analysis is needed to determine the knee angle.

To test the sensor's performance, we simultaneously tracked the temporal evolution of the knee angle with the calibrated fiber-based device and by visual motion capture, while a subject was walking and running on a treadmill (Figure 4c, and Supporting Information, Video 1). The angle data captured in real-time with our sensor closely matched the data resulting from post-experimentation analysis of the collected video stream. The results suggest that our portable, wireless fiber-based knee angle monitoring device could allow for the real-time monitoring of body kinematics to aid in rehabilitation, assess athletic performance, and design of equipment that supports or enhances human walking.

In a second application, we targeted the accurate quantification of hand movement and its transfer to human-machine interfacing. We designed a glove that incorporated a fiber-based deformation sensor for each finger (Figure 4d), using the same conceptual design as for the knee brace. We verified the correct function of the finger position-sensing glove by simultaneously capturing the sensor output and video recording the position of the five fingers while performing various hand gestures (Figure 4e). Specific gestures that rely on fully extended or bent fingers can easily be captured with our sensing glove. To assess how accurately the device can capture intermediate finger configurations, we created a virtual 3D hand model that we controlled in real-time with the glove (Supporting information, Video 2). As is shown in the video, the continuous motion of each individual finger is mimicked faithfully in real-time by the virtual hand. Thus, we anticipate that this finger-position sensing glove could be employed to intuitively interact with a virtual environment or to control internet-of-things devices. For a playful demonstration, we associated each finger of the virtual model with a piano key, which is triggered and released by flexing and relaxing the finger by a

specific amount. This allowed us to play simple “air piano” tunes with the glove (Supporting Information, Video 3).

Finally, to demonstrate that this fiber-based sensing scheme can also be applied to locate deformations, we designed a tennis racket that provides feedback about ball impact location (Figure 4f), which governs both speed and accuracy of the shot. The racket features a 3-by-3 mesh of fibers arranged atop the racket strings, each connected to its respective LED and photodiode. The impact of a ball in a specific location on the racket indents just the fibers present in that location, resulting in a dip in the transmitted light intensity, which locates the impact. A ball was bounced off the racket repeatedly, while the transmission strength of all fibers was monitored at a sample rate of 184 Hz (Figure 4g). Fibers that were hit by the ball showed a significantly more pronounced dip in transmission (visualized by a peak in attenuation in Figure 4g) than other fibers that are just experiencing vibrations. This simple set-up permits localization of the ball impact with remarkable accuracy (Supporting Information, Video 4), enabling applications in data-supported training, analysis, and statistics.

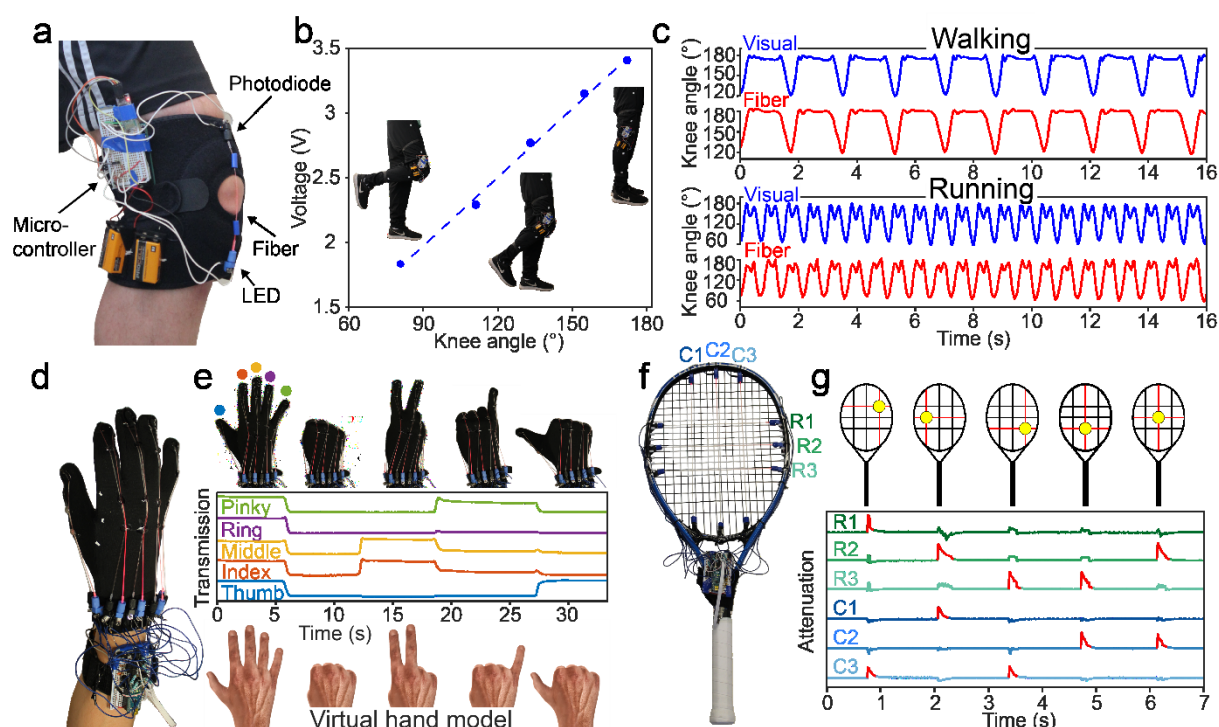


Figure 4. Fibers in human activity monitoring. (a) A fiber-based sensor, including a LED and a photodiode, is integrated in a knee brace for the monitoring of knee movement. (b) The measured sensor response can be approximated by a linear function of the true knee bending angle, measured with visual motion capture. (c) Knee angle during walking and running of a test subject determined by both the fiber-based device and visual motion capture. (d) Glove featuring a fiber-based sensor on each finger for the capture of hand movement. (e) Hand gestures (illustrated by the photographs above the graph) are identified based on the output of the sensors and visualized in real-time by a virtual hand model on a computer (shown below the graph). (f) A mesh of 3-by-3 fiber-based sensors is integrated in a tennis racket. (e) Inverted normalized signal for each of the six fibers in the racket. The peaks are highlighted in red. Based on the sensor signals, the location of the impact of a ball can be automatically determined.

3. Conclusion

We have demonstrated the scalable fabrication of highly stretchable step-index core-cladding optical fibers made of low-cost thermoplastic elastomers using a one-step co-extrusion process. The fibers guide light (attenuation coefficient 0.8 dB cm^{-1}) and can sustain extreme deformations (elongation at

break 545%). Stretching, bending, and indentation of the fibers results in predictable, repeatable, and reversible transmission losses, as we have shown for 100 deformation cycles, where fibers were repeatedly subjected to strains of 300%. To our knowledge, no other reported stretchable optical fiber system performs reliably at such extreme magnitudes of strain. To demonstrate the fibers' utility for challenging mechanical sensing applications, we constructed three fully-integrated, stand-alone, wirelessly-communicating sensing systems: a knee brace for monitoring knee movement during walking and running, a glove for tracking finger movement in real-time, and an impact sensor in a tennis racket. These examples show that the fibers' opto-mechanical properties and their reliable performance during repeated exposure to large strains and high-speed impacts are valuable attributes for mechanically demanding sensing scenarios, such as the monitoring of human motion in real-time with excellent precision and time resolution.

The fibers form a versatile material platform for the design of advanced sensing devices in health monitoring, rehabilitation, physical training, human-machine interaction, advanced functional textile design, and control of internet-of-things devices.

4. Experimental Section

Polymer Comparison: All procured thermoplastic elastomers (Sigma Aldrich Polystyrene-block-polyisoprene-block-polystyrene; Star Clear 1003, 1025, and 1044; Polymax TPE C4900; Ineos Styrolution 2G66 and 3G46; Daikin T-530; 3M Dyneon 221GZ and 2030GZ) were compared using the metrics elongation at break and refractive index. Values were taken from the data sheets for the elongation at break for all materials and for the refractive index for materials supplied by Ineos

Styrolution, Daikin, and Dyneon. The refractive indices of all remaining materials were determined experimentally using reflectometry of thin films (Supporting Information, Figure S5).

Fiber Manufacture: Two single-screw extruders (Filastruder, Filabot) were connected using a custom co-extrusion nozzle. Polymer granules of the core (Star Clear 1044) and cladding material (Daikin T-530) were fed to the two separate extruders, where they were conveyed forward, molten down, and ultimately co-centrally combined in the nozzle. The temperature of the core and cladding extruder, and co-extrusion nozzle were set to 180 °C, 340 °C, and 300 °C, respectively. Downstream, the core-cladding fiber was taken up by a spool with speed-control, enabling tuning of the fiber diameter.

Structural, Mechanical, and Optical Analysis: The fiber end faces were examined by light microscopy (Olympus BX51). The mechanical behavior of the fibers was determined by static and dynamic tensile testing. Static tensile tests were performed on a standard frame (Instron 5860; clamped fiber section 20mm; speed 1 mm min⁻¹). Dynamic tensile tests were carried out using a custom stretching setup including a low-force load cell (LCM Systems UF1; clamped fiber section 100mm; speed 1 mm min⁻¹). In all transmission measurements, light from a white light source (Thorlabs SLS201) was coupled in the stretchable optical fibers and the transmitted light analyzed using a spectrometer (Ocean Optics Maya 2000 Pro) in the wavelength range 400 nm – 1000 nm. In the cutback experiment, the fibers were sequentially trimmed by 5mm using a razor blade and the transmission spectrum recorded for each fiber length. For assessing the effect of the surrounding medium, the transmission spectra of suspended fibers (length 15mm) in air, and subsequently with a fiber section

(10mm) submerged in de-ionized water and silicone oil (Alfa Aesar A12728), were measured. A single transmission value for each fiber and medium was obtained by integrating the transmission spectrum in the wavelength range 400 nm – 1000 nm. The relative transmission was calculated with the ratio of transmission in water/silicone oil to air. In the mechano-optical tests, the fibers were sequentially deformed using a custom setup and the transmission spectrum measured after each deformation step (total fiber length 200mm, deformed length 100mm). For indentation, a metal rod with a diameter of 6mm positioned perpendicularly to the fiber served as an indenter. Step sizes of fiber extension, bending radius, and indentation depth were set to 10mm, 0.5mm, and 0.0625mm, respectively.

Fiber-based sensors testing: The design and fabrication of all fiber-based devices is described in the Supporting Information. For the fiber-based knee brace, the signal was compared to the true knee bending angle obtained by visual motion tracking. For this, reflective markers were fixed on the side of a subject's upper and the lower leg and their positions were tracked during knee motion using video capture and analysis (Open Source Physics Tracker). Based on the relative position of the markers, the true knee angle was calculated. We found an approximately linear decrease of sensor output voltage as a function of true knee angle (Figure 4b). The slope and intercept of the linear relation between knee angle and sensor output voltage vary based on the person and the positioning of the brace on the knee, requiring calibration of the device. This can easily be accomplished on-site immediately before device operation using only two visually estimated knee angles (90° and 180° were used in the subsequent tests presented in Figure 4c) with which the linear

calibration function can fully be determined. The fiber-based glove was calibrated accordingly using two finger configurations (fully extended and fully bent).

Supporting Information

Supporting Information is available from the Wiley Online Library or from the author.

Acknowledgements

The authors thank Pierce Hayward for tensile testing support, Stephen Banzaert for helpful pointers for the electrical design of the sensor devices, Ben Miller for software development, and Janille Maragh for inspiring discussions. A.L. acknowledges the financial support from the German Academic Exchange Service (DAAD PROMOS scholarship) and the Elite Master's Program in Advanced Materials and Processes at Friedrich-Alexander University Erlangen-Nürnberg. M.K. acknowledges support by the National Science Foundation through the 'Designing Materials to Revolutionize and Engineer our Future' program (DMREF-1533985).

((Acknowledgements, general annotations, funding. Other references to the title/authors can also appear here, such as "Author 1 and Author 2 contributed equally to this work."))

Received: ((will be filled in by the editorial staff))

Revised: ((will be filled in by the editorial staff))

Published online: ((will be filled in by the editorial staff))

References

This article is protected by copyright. All rights reserved.

- [1] J. De jonckheere, F. Narbonneau, M. Jeanne, D. Kinet, J. Witt, K. Krebber, B. Paquet, A. Depre, R. Logier, in *2009 Annu. Int. Conf. IEEE Eng. Med. Biol. Soc.*, IEEE, **2009**, pp. 1473–1476.
- [2] R. T. Gibbs, H. H. Asada, *J. Neuroeng. Rehabil.* **2005**, *2*, 7.
- [3] O. Atalay, W. R. Kennon, E. Demirok, *IEEE Sens. J.* **2015**, *15*, 110.
- [4] D. Z. Stupar, J. S. Bajic, L. M. Manojlovic, M. P. Slankamenac, A. V. Joza, M. B. Zivanov, *IEEE Sens. J.* **2012**, *12*, 3424.
- [5] R. P. Rocha, A. F. Silva, J. P. Carmo, J. H. Correia, in *2011 Annu. Int. Conf. IEEE Eng. Med. Biol. Soc.*, IEEE, **2011**, pp. 458–461.
- [6] C. Perez-Ramirez, D. Almanza-Ojeda, J. Guerrero-Tavares, F. Mendoza-Galindo, J. Estudillo-Ayala, M. Ibarra-Manzano, *Sensors* **2014**, *14*, 24483.
- [7] A. F. da Silva, A. F. Goncalves, P. M. Mendes, J. H. Correia, *IEEE Sens. J.* **2011**, *11*, 2442.
- [8] E. Fujiwara, D. Y. Miyatake, M. Ferreira, C. K. Suzuki, in *Human-Robot Interact.*, **2013**, pp. 123–124.
- [9] T. Yamada, Y. Hayamizu, Y. Yamamoto, Y. Yomogida, A. Izadi-Najafabadi, D. N. Futaba, K. Hata, *Nat. Nanotechnol.* **2011**, *6*, 296.
- [10] M. Amjadi, A. Pichitpajongkit, S. Lee, S. Ryu, I. Park, *ACS Nano* **2014**, *8*, 5154.
- [11] A. Atalay, V. Sanchez, O. Atalay, D. M. Vogt, F. Haufe, R. J. Wood, C. J. Walsh, *Adv. Mater. Technol.* **2017**, *2*, 1700136.
- [12] C. B. Cooper, K. Arutselvan, Y. Liu, D. Armstrong, Y. Lin, M. R. Khan, J. Genzer, M. D. Dickey, *Adv. Funct. Mater.* **2017**, *27*, 1605630.
- [13] S. W. Park, P. S. Das, A. Chhetry, J. Y. Park, *IEEE Sens. J.* **2017**, *17*, 1.
- [14] R. Wijesiriwardana, *IEEE Sens. J.* **2006**, *6*, 571.
- [15] B. M. Quandt, L. J. Scherer, L. F. Boesel, M. Wolf, G.-L. Bona, R. M. Rossi, *Adv. Healthc. Mater.* **2015**, *4*, 330.
- [16] W. Zeng, in *Handb. Smart Text.*, Springer Singapore, Singapore, **2015**, pp. 109–125.
- [17] I. Martincek, D. Pudis, M. Chalupova, *IEEE Photonics Technol. Lett.* **2014**, *26*, 1446.
- [18] J. Guo, M. Niu, C. Yang, *Optica* **2017**, *4*, 1285.

- [19] H. Zhao, K. O'Brien, S. Li, R. F. Shepherd, *Sci. Robot.* **2016**, *1*, eaai7529.
- [20] M. Choi, M. Humar, S. Kim, S. H. Yun, *Adv. Mater.* **2015**, 4081.
- [21] J. Guo, X. Liu, N. Jiang, A. K. Yetisen, H. Yuk, C. Yang, A. Khademhosseini, X. Zhao, S. Yun, *Adv. Mater.* **2016**, *28*, 10244.
- [22] M. Rothmaier, M. P. Luong, F. Clemens, *Sensors* **2008**, *8*, 4318.
- [23] M. Krehel, R. Rossi, G. Bona, L. Scherer, *Sensors* **2013**, *13*, 11956.
- [24] M. Krehel, M. Schmid, R. Rossi, L. Boesel, G. Bona, L. Scherer, *Sensors* **2014**, *14*, 13088.
- [25] C. K. Harnett, H. Zhao, R. F. Shepherd, *Adv. Mater. Technol.* **2017**, *2*, 1700087.
- [26] O. Ziemann, J. Krauser, P. E. Zamzow, W. Daum, *POF Handbook*, Springer Berlin Heidelberg, **2008**.
- [27] B. C. Goswami, R. D. Anandjiwala, D. Hall, *Textile Sizing*, CRC Press, **2004**.
- [28] J. Diani, B. Fayolle, P. Gilormini, *Eur. Polym. J.* **2009**, *45*, 601.
- [29] H. Cho, S. Mayer, E. Pösel, M. Susoff, P. J. in 't Veld, G. C. Rutledge, M. C. Boyce, *Polymer (Guildf)*. **2017**, *128*, 87.
- [30] K. Kalli, D. J. Webb, in *Adv. Fiber Opt.*, **2011**, pp. 345–388.
- [31] C. Lu, S. Park, T. J. Richner, A. Derry, I. Brown, C. Hou, S. Rao, J. Kang, C. T. Mortiz, Y. Fink, P. Anikeeva, *Sci. Adv.* **2017**, *3*, e1600955.
- [32] J. Zubia, J. Arrue, *Opt. Fiber Technol.* **2001**, *7*, 101.

Stretchable and flexible step-index optical fibers made of melt-processible thermoplastic elastomers are used for deformation sensing. Stretching, bending, and indentation of the fibers induce detectable, predictable, reversible, and wavelength-dependent changes in light transmission. Fiber-based optical sensors capable of reliably quantifying extreme mechanical stimuli, such as axial strains of 300%, are employed in human activity monitoring.

Keywords: stretchable optical fibers, human motion tracking, textile-based sensors, thermoplastic elastomers, soft optical materials

Andreas Leber, Beth Cholst, Joseph Sandt, Nicolas Vogel & Mathias Kolle*

Stretchable Thermoplastic Elastomer Optical Fibers for Sensing of Extreme Deformations

